Persistent Photoconductivity in Chemically Modified Single-Wall Carbon Nanotubes

Rafail F. Khairoutdinov,*,† Larissa V. Doubova,† Robert C. Haddon,‡ and Laxmikant Saraf§

Department of Chemistry and Biochemistry and Center for Nanosensor Technology, University of Alaska−Fairbanks, Fairbanks, Alaska 99775-6160, Department of Chemistry, University of California−Riverside, Riverside, California 92521-0403, and WR Wiley Environmental Molecular Sciences Laboratory, Pacific Northwest National Laboratory, Richland, Washington 99352

Received: August 4, 2004; In Final Form: September 3, 2004

Control of the conductivity of single wall carbon nanotubes (SWNTs) is crucial for the use of carbon nanotubes in molecular electronics. We report a new fundamental characteristic of semiconducting SWNTs: the persistent photoconductivity of chemically modified carbon nanotube films. Illumination of carboxylated semiconducting SWNTs with ultraviolet or visible light causes a persistent decrease in the conductivity of semiconducting films. The photoinduced conductivity persists in the dark with a characteristic half-life of 35 s to 1.2×10^3 s at room temperature and an activation energy of 0.35 eV. Infrared illumination restores the conductivity of SWNT films. Ultraviolet and visible light illumination partially refills empty valence band states of chemically modified SWNTs by electron injection from the dopant sites. Photoinduced injection of electrons is accompanied by a decrease of the conductivity of the *p*-doped SWNT film, because of neutralization of holes by injected electrons. Covalent attachment of ruthenium(II)-tris(2,2′-bipyridine) ($Ru(bpy)_3^{2+}$) to SWNTs makes carbon nanotubes sensitive to light that has been absorbed by the ruthenium complex and makes the carbon nanotubes persistently photoconductive. The photoconductivity of $Ru(bpy)_3^{2+}$−SWNT films is presumably due to the injection of holes from $*Ru(bpy)_3^{2+}$ to SWNT with a quantum yield of 0.55. Persistently photoconductive SWNTs have potential uses as nanosized optical switches, photodetectors, electrooptical information storage devices, and chemical sensors.

Introduction

Unique electronic properties and dimensions make single-wall carbon nanotubes (SWNTs) ideal building blocks for molecular electronics devices. A variety of basic SWNT-based molecular-scale electronic devices (such as molecular wires, diodes, and field-effect and single-electron transistors) have recently been constructed.[1−5] One of the challenges in the development of molecular electronics is to integrate such devices onto a chip and control the flow of electrons between individual components. Also, the detailed electron transport properties of semiconducting SWNTs must be clarified.

Both semiconducting and metallic SWNTs normally co-exist, even within a single carbon nanotube bundle, and their separation is difficult.[6] Photoconductivity studies allow one to characterize the semiconducting SWNTs within a mixture of semiconducting and metallic nanotubes.[7,8] Light also offers a simple, precise, and convenient tool for switching electrical circuits.[9] Many fundamental processes such as photoconductivity and exciton formation, inner- and outer-sphere electron transfer of excited molecules, and photosynthesis include photoinduced charge separation as a key reaction. It also has a fundamental role in artificial systems for solar energy conversion.[10,11] Here, we report that photoinduced charge separation within chemically modified semiconducting SWNTs is followed by a persistent change in the conductivity of carbon nanotube films. The photoinduced conductivity persists in darkness, with a characteristic half-life of 35 s to 1.2×10^3 s at room temperature and an activation energy of 0.35 eV.

We have previously reported that ultraviolet illumination of carboxylated SWNTs results in the filling of valence band states of the semiconducting SWNTs. This process presumably includes reduced dopants—defective oxidized carbon sites, together with holes in the band electronic structure, that are inevitably generated during the purification of SWNTs by a strong acid treatment.[12] Acid purification results in *p*-doping of semiconducting SWNTs.[12−14] Therefore, changes in the SWNT valence band population might alter SWNT conductivity, thus making light modulation of their electrical conductivity possible. However, the concentration of dopants, and hence the efficiency of light-induced population changes, is dependent on the acid treatment protocol and thermal history of the sample, thus making the control of the photoconductivity characteristics of SWNT quite difficult. We show here that covalent attachment of $Ru(bpy)_3^{2+}$ to the SWNT surface makes the carbon nanotube selectively light-sensitive, and that illumination of $Ru(bpy)_3^{2+}$−SWNT in the characteristic $Ru(bpy)_3^{2+}$ absorption band results in a persistent increase in conductivity of the semiconducting SWNT film.

Experimental Section

In the experiments, we have used electric-arc-produced SWNTs that were provided by Carbon Solutions, Inc.[15] After purification and carboxylation of the SWNT by nitric acid,[16,17] the relative purity of SWNT was evaluated to be 90% against an R2 standard.[12]

a. Synthesis of the 4′-Methyl-2,2′-bipyridine-4-carboxylaldehyde.[18,19] SeO_2 (1.74 g) was added to a solution of 4,4′-

* Author to whom correspondence should be addressed. Telephone: 907-474-7654. Fax: 907-474-5640. E-mail address: ffrk@uaf.edu.
† University of Alaska Fairbanks.
‡ University of California−Riverside.
§ Environmental Molecular Sciences Laboratory.

10.1021/jp046495m CCC: $27.50
Published on Web 12/01/2004

dimethyl-2,2′-bipyridine (2.64 g) in 75 mL of dioxane and refluxed for 24 h.

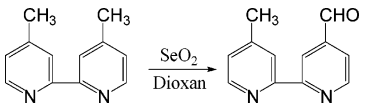

The solution was filtered hot and the solvent was removed from the filtrate by rotary evaporation. The residue was dissolved in ethyl acetate and filtered, to remove additional solid material. The ethyl acetate layer was extracted with 1 M Na_2CO_3 (2 × 100 mL) to remove additional carboxylic acid and 0.3 M $Na_2S_2O_5$ (3 × 100 mL) to form the aldehyde bisulfite. The combined aqueous extracts were adjusted to pH 10 with Na_2CO_3 and extracted with CH_2Cl_2 (4 × 100 mL). The organic phases containing 4′-methyl-2,2′-bipyridine-4-carboxylaldehyde were collected and evaporated.

The yield was 1.61 g (57%), in the form of a white powder. The melting point (mp) was 131 °C.

b. Synthesis of 4′-Methyl-2,2′-bipyridine-4-carboxylic acid (cbpy).[20] A solution of $AgNO_3$ (1.44 g) in 15 mL of water was added to a suspension of 4′-methyl-2,2′-bipyridine-4-carboxylaldehyde (1.61 g) in 69 mL of 95% ethanol.

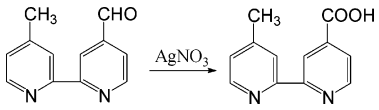

The suspension was stirred rapidly and 37 mL of 1 M NaOH was added dropwise over 20 min to form Ag_2O. The black solution was stirred for an additional 15 h. The ethanol was removed by rotary evaporation, and the remaining solution was filtered to remove Ag_2O. The residue was washed with 1.3 M NaOH (2 × 20 mL) and 20 mL of H_2O. The combined filtrates were extracted with CH_2Cl_2 to remove unreacted aldehyde and adjusted to pH 3.5 with 1:1 (v/v) 4 N HCl:AcOH to give a white compound. The product precipitated overnight at −10 °C, and the compound was collected.

The yield was 1.16 g (64%), in the form of a white powder. The melting point (mp) was 280 °C. ^{1}H NMR ($CDCl_3$, 300 MHz): δ 2.5 (s, 3 H); 7.15−9 (m, 6 H).

c. Synthesis of Ruthenium(II)-bis(2,2′-bypiridine)−(4′-Methyl-2,2′-bipyridine-4-carboxylic acid)-bis(hexafluorophosphate) Ru(bpy)$_2$(cbpy)$^{2+}$.[20] $Ru(bpy)_2Cl_2$ (0.9 g) was added to a solution of 4′-methyl-2,2′-bipyridine-4-carboxylic acid (0.45 g) in 75 mL of 70% ethanol/water and refluxed for 21 h.

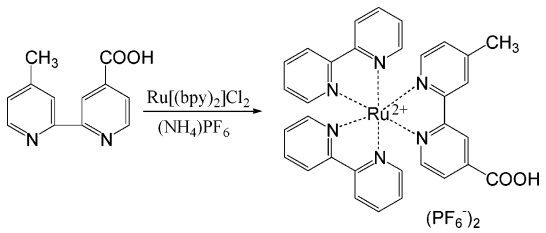

The reaction mixture was cooled and ethanol was removed under vacuum. After the solution was allowed to stand for 4 h at room temperature, it was filtered and the solid compound obtained was washed with cold water. The filtrate was treated with a saturated aqueous solution of NH_4PF_6 until no further precipitate was observed. The mixture was kept at room temperature for an additional 2 h and then was filtered and washed with cold water and ether. The solid was dried overnight.

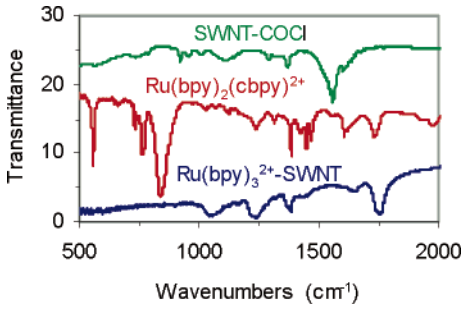

Figure 1. Infrared spectra of SWNT−COCl (green), $Ru(bpy)_2(cbpy)^{2+}$ (red), and $Ru(bpy)_3^{2+}$−SWNT (blue). Spectra of SWNT−COCl and $Ru(bpy)_2(cbpy)^{2+}$ are shifted vertically, with respect to the spectrum for $Ru(bpy)_3^{2+}$−SWNT.

The yield was 1.0 g (65%), in the form of an orange powder. The material has characteristic absorption and fluorescence bands at 287, 456, and 608 nm, respectively.

d. Synthesis of Ruthenium(II)-bis(2,2′-bypiridine)−(4′-Methyl-2,2′-bipyridine-4-carboxylic-carboxylic−SWNT Anhydride) (Ru(bpy)$_3^{2+}$−SWNT). A quantity of carboxylated SWNTs (56 mg) was mixed under vigorous stirring with 11.2 mL of $SOCl_2$ and three drops of dimethylformamide (DMF). The mixture was maintained, with stirring, at 70 °C for 20 h and then unreacted $SOCl_2$ was removed under vacuum. The solid SWNT−COCl was dried under vacuum overnight.

SWNT−COCl (10 mg) was sonicated for 5 min in 5 mL of anhydrous DMF and then mixed with a sodium salt of $Ru(bpy)_2(cbpy)^{2+}$ (50 mg) with stirring. The reaction mixture was maintained at 100 °C under argon for 15 h. The product was then filtered, to remove the solvent. The black material was then repeatedly washed with anhydrous ethanol and CH_2Cl_2.

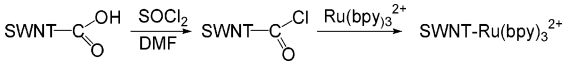

IR spectra of the SWNT−COCl, $Ru(bpy)_2(cbpy)^{2+}$, and $Ru(bpy)_3^{2+}$−SWNT measured in the solid state are presented in Figure 1. This figure shows the shift of the C═O carbonyl vibration from 1732 cm^{-1} to 1750 cm^{-1}, which is indicative of the anhydride formation, and a new band at 1050 cm^{-1}, which is characteristic of the C═O stretch in functionalized SWNTs.[21] Figure 1 also shows that the intense absorbance increases as the frequency decreases below 800 cm^{-1}, because of defects and impurity states introduced into SWNTs by chemical modification.[12,13]

Thin films of SWNTs were prepared by spraying the dispersions on heated microscope glass slides (200 °C, DMF). Four thin (150-nm-thick) 3-mm-wide co-planar copper/nickel contacts (2 mm away from each other) were deposited on the films. Film conductivity was measured using a Keithley model 2000 multimeter. To prevent moisture condensation on the SWNT film, conductivity measurements were performed in a sealed glass cell that was placed in a thermostated bath. Film temperature was controlled by a thermocouple that was attached to the film, which was supported by a glass slide surface. Temperature fluctuations did not exceed ±1 °C. Film deoxygenation was achieved by blowing argon through a sealed quartz cuvette that contained a film for 20 min.

Continuous photolysis experiments were performed using a xenon lamp light that was filtered with glass filters. Light intensities were measured using a calibrated PowerMax 500D laser power meter. Optical spectra were recorded using a Nicolet Magna-IR 560 E.S.P. IR spectrometer and a Varian Cary 500 double beam scanning UV/Vis/NIR spectrophotometer. Emis-

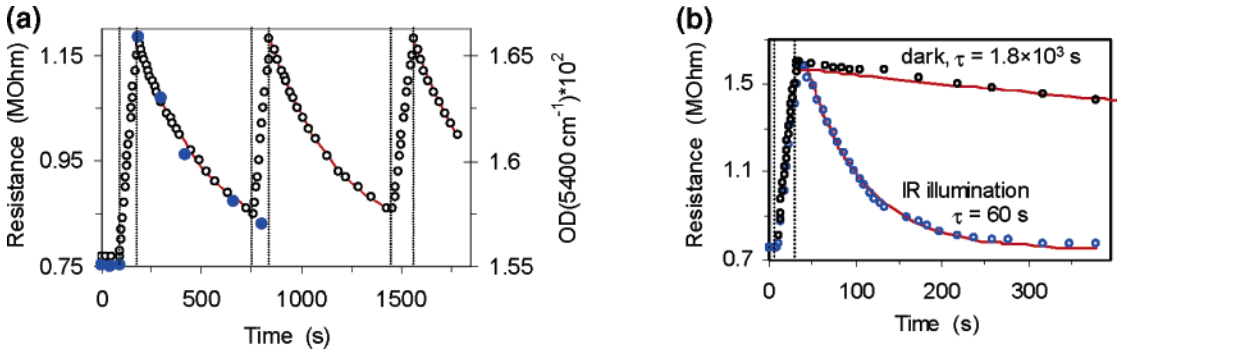

Figure 2. Resistance (open circles) and absorbance (solid circles) of the carboxylated SWNT film. Dotted lines separate intervals when the film was kept in darkness (no changes or decay) and under UV illumination. Panel a shows ultraviolet illumination with a xenon lamp (220 nm $< \lambda <$ 400 nm, intensity $I = 0.023$ W/cm^2); solid lines show an exponential fit of experimental data with $\tau = 340$ s. Panel b shows full light illumination with a xenon lamp ($I = 0.15$ W/cm^2), followed by keeping sample in darkness or under illumination with an infrared lamp ($\lambda > 720$ nm, $I = 1.6$ W/cm^2).

sion spectra were recorded using a Perkin−Elmer model LS-50B spectrofluorimeter.

Results and Discussion

SWNT films consist of a network of semiconducting and metallic nanotubes. If the density of metallic nanotubes exceeds the percolation threshold, then the network becomes metallic. Below that critical density, SWNT films demonstrate semiconducting characteristics. We found that thin films with an absorbance of <0.1 at the characteristic wavenumber of 5400 cm^{-1} (the first interband transition (S_{11}) of semiconducting SWNTs) have a resistance that exceeds 10^5 Ω, but the resistance decreases to <500 Ω for thick films with an absorbance at 5400 cm^{-1} of Abs(5400 cm^{-1}) > 1. No effect of light on the conductivity was observed for the thick SWNT films. These observations indicate the semiconducting nature of the thin films and the metallic nature of the thick samples.

Figure 2a shows the photoinduced changes in absorbance at 5400 cm^{-1} of a thin film of carboxylated SWNTs. UV illumination of semiconducting SWNTs has been observed to partially refill empty valence band states, presumably by the injection of electrons from the dopant sites. Photoinduced injection of electrons is accompanied by a decrease of the conductivity of the SWNT film; presumably, this negative photoconductivity is due to neutralization of holes (denoted hereafter by the superscripted symbol "⊕") by injected electrons, which is a well-known phenomenon for bulk *p*-type semiconductors:[22]

$$\mathrm{SWNT}^{n\oplus} + m\mathrm{DS}^- \xrightarrow{\text{UV light}} \mathrm{SWNT}^{(n-m)\oplus} + m\mathrm{DS}^\circ$$

where DS° and DS$^-$ denote the oxidized dopant and its reduced form, respectively.

The S_{11} absorbance change and photoinduced resistance enhancement of semiconducting SWNT films continuously decreases as the wavelength of illuminating light increases; practically no changes were observed at >550 nm. Illumination of the film with the full light of a xenon lamp increases the resistance rise rate.

Slow back-reduction of defective oxidized carbon sites by electrons from the valence band is responsible for the decay in the S_{11} absorbance in darkness (see Figure 2a).[23] Correspondingly, the resistance of the film decreases exponentially, with a decay time up to $\tau = 1.8 \times 10^3$ s (see Figure 2a and 2b). Different spatial distributions of recombining emptied oxidized carbon sites and valence band electrons under different illumination conditions might be a reason for the different dark decay times in Figure 2a and 2b.

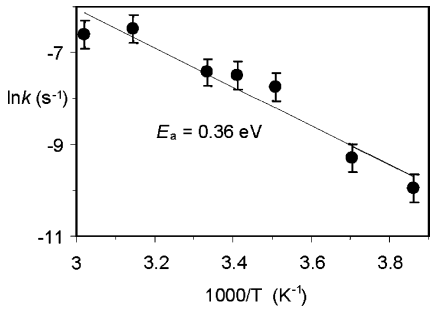

Figure 3. Temperature dependence of the photoinduced resistance decay rate of the carboxylated SWNT film. Solid line is the result of the fit with an activation energy of $E_a = 0.36$ eV.

The infrared illumination of the film with a wavelength of $\lambda > 720$ nm quenches the photoinduced resistance, decreasing the characteristic time of the resistance decay to $\tau = 60$ s. These observations and the reduction of the S_{11} absorbance at infrared illumination of SWNT films[23] indicate the following mechanism for the thermal and IR quenching of SWNT films conductivity:

$$\mathrm{SWNT}^{(n-m)\oplus} \xrightarrow{kT,\ \text{IR light}} \mathrm{SWNT}^{n\oplus} + m\mathrm{DS}^-$$

The infrared illumination results in the excitation of electrons from the valence band to the conduction band, followed by a transfer of electrons from the conduction band to the defective oxidized carbon sites.

The activation energy of the thermal electron transfer from the valence band to the dopant sites was determined from the temperature dependence of the resistance decay rate. Figure 3 shows the temperature dependence of the resistance decay rate of the carboxylated SWNT film. The best fit of the experimental data corresponds to the following activation energy: $E_a = 0.36 \pm 0.01$ eV.

The attachment of $Ru(bpy)_3^{2+}$ to SWNT (see Figure 4a) did not change the behavior of the semiconducting films under UV illumination. Similar to carboxylated SWNT films, the conductivity of the ($Ru(bpy)_3^{2+}$−SWNT) films decreased under UV illumination. However, illumination of these films in the characteristic $Ru(bpy)_3^{2+}$ visible absorption band (440 nm < λ_{illum} < 520 nm) resulted in an increase in the film conductivity (see Figure 4b).[24] The dynamics of the conductivity changes indicates that the visible illumination of $Ru(bpy)_3^{2+}$−SWNT generates holes in the film, presumably via electron transfer from the SWNT itself to the photoexcited $Ru(bpy)_3^{2+}$, followed by a slow back-recombination process in darkness:

$$\mathrm{Ru(bpy)_3}^{2+}\text{−SWNT} \underset{kT}{\overset{h\nu}{\rightleftharpoons}} \mathrm{Ru(bpy)_3}^{+}\text{−SWNT}^{\oplus}$$

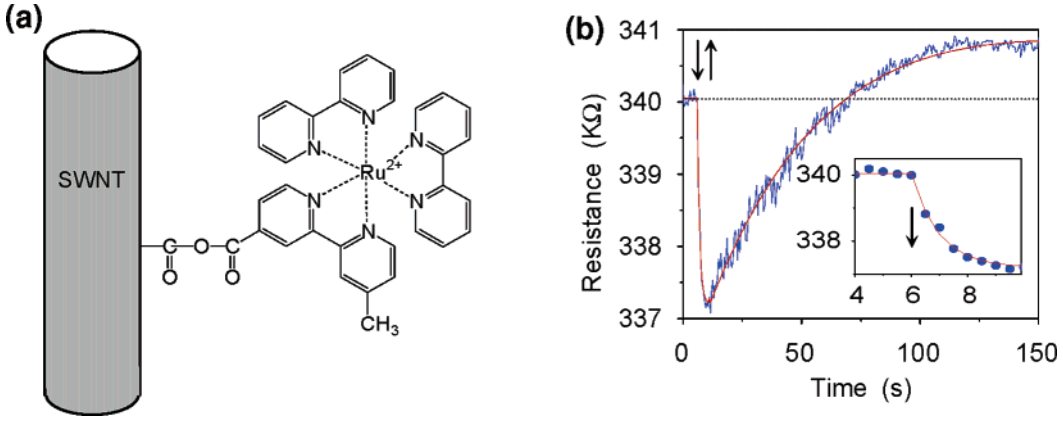

Figure 4. (a) Structure of ruthenium(II)-bis(2,2′-bipyridine)−(4′-methyl-2,2′-bipyridine-4-carboxylic-carboxylic−SWNT anhydride) ($Ru(bpy)_3^{2+}$−SWNT). (b) Dynamics of resistance changes under illumination by visible light (440 nm $< \lambda <$ 520 nm, $I = 0.015$ W/cm^2) of the $Ru(bpy)_3^{2+}$−SWNT film. The concentration of $Ru(bpy)_3^{2+}$ moieties is 2×10^{11}/cm^2. Vertical arrows indicate light-on (↓) and light-off (↑) events. The initial portion of the resistance changes is shown in the inset, together with an exponential fit with $\tau_p = 1 \pm 0.05$ s. Blue lines and circles denote experimental data, and red lines represent results of the fit.

Thus, two major processes are occurring upon visible illumination of the $Ru(bpy)_3^{2+}$-modified SWNTs. Similar to carboxylated SWNT films, visible illumination of $Ru(bpy)_3^{2+}$−SWNT films causes an injection of electrons from the dopants into the SWNT holes. Visible illumination also generates holes in SWNT via a withdrawal of electrons from nanotubes by $*Ru(bpy)_3^{2+}$. These two effects explain why the photoconductivity of $Ru(bpy)_3^{2+}$−SWNT film in Figure 4 first increases and then, in darkness, decreases to become lower than it was before illumination. Under visible illumination, hole injection into SWNTs ultimately prevails over the photoinjection of electrons from dopants into SWNT holes, and the film photoconductivity is observed. In darkness, back-electron transfer from $Ru(bpy)_3^{+}$ to SWNT seems to be faster than the refilling of the SWNT holes. As a result, the remaining photoinjected electrons eventually outnumber the remaining photoinduced holes, and the conductivity decreases below the initial level. According to Figure 4, it happens at a time $t \approx 70$ s, when the resistance of the $Ru(bpy)_3^{2+}$−SWNT film becomes higher than it was before illumination.

Assuming that the dark conductivity decay is a superposition of these two exponential processes, the rate constants for electron transfer from $Ru(bpy)_3^{+}$ to SWNT and from the valence band of the nanotube to the defect sites of SWNT that give the best fit to experimental data are $(2 \pm 0.2) \times 10^{-2}$ s^{-1} and $(3 \pm 1) \times 10^{-3}$ s^{-1}, respectively.

Persistent photoconductivity of semiconducting materials occurs in group II−VI compounds,[25] group III−V ternary alloys,[26,27] and irradiated silicon and germanium,[28] and this feature is of interest because of its potential applications in optoelectronic devices.[29,30] Persistent photoconductivity can provide a substantial increase of the superconducting critical temperature[31] and can lead to the formation of superconducting filaments in otherwise insulating materials.[32] The physical mechanisms responsible for these effects are still under debate. However, two general mechanisms for persistent photoconductivity of semiconducting materials have been identified. The most common involves a large relaxation of the lattice around impurity centers when a photoelectron is released.[33] The second model is based on the spatial separation of the photogenerated electrons and holes by macroscopic potential barriers caused by band bending at planar surfaces, interfaces, and junctions, or around doping inhomogeneities. If these potential barriers are sufficiently high, the lifetimes of the persistent electrons and holes become very long.[34]

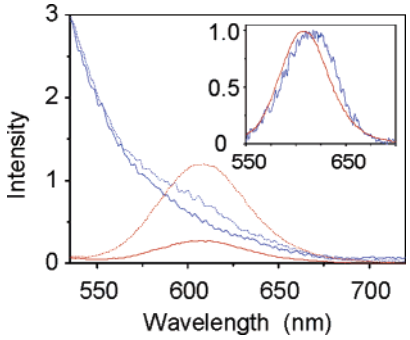

Figure 5. Luminescence spectra of $Ru(bpy)_3^{2+}$ (red) and $Ru(bpy)_3^{2+}$−SWNT (blue) at $\lambda_{ex} = 465$ nm in air-saturated (solid lines) and argon-saturated (dashed lines) dimethylformamide (DMF). Spectra are normalized to the specific absorption of $Ru(bpy)_3^{2+}$ at 460 nm. Difference (argon versus air) luminescence spectra are shown in the inset. Spectra are normalized to the emission intensity at the maximum.

The nature of persistent photoconductivity of *p*-doped semiconducting SWNT is still to be determined. For $Ru(bpy)_3^{2+}$−SWNT films, the low rate of electron transfer from $Ru(bpy)_3^{+}$ to the carbon nanotube might be caused by the anhydride spacer arm and an unfavorable mutual orientation of $Ru(bpy)_3^{+}$ and SWNT that occurs after photoinduced electron transfer.[35] One of the reasons for the persistent negative photoconductivity of carboxylated SWNT films may be the large delocalization of valence band electrons in SWNT, which causes an unfavorable increase in entropy as electrons are transferred from the valence band to the defect oxidized carbon sites. This slows the rate of dark electron transfer from the valence band states of SWNT to dopant sites.

To characterize the persistent photoconductivity of $Ru(bpy)_3^{2+}$−SWNT films quantitatively, we have studied $Ru(bpy)_3^{2+}$ luminescence quenching by SWNT. $Ru(bpy)_3^{2+}$ solution in DMF has a characteristic emission band at 608 nm (see Figure 5). The emission spectrum of $Ru(bpy)_3^{2+}$−SWNT demonstrates a featureless band that is characteristic of SWNT solutions, indicating a quenching of the $Ru(bpy)_3^{2+}$ excited state by SWNT. The removal of oxygen from the solution significantly increases the intensity of $*Ru(bpy)_3^{2+}$ luminescence and reveals the emission of $*Ru(bpy)_3^{2+}$−SWNT. As the inset in Figure 5 shows, the emission maximum of $Ru(bpy)_3^{2+}$ attached to SWNT is red-shifted by ∼6 nm, relative to the emission maximum of nonbonded $Ru(bpy)_3^{2+}$. An analogous shift was previously observed for a merocyanine form of spiropyran that

was attached to a SWNT.[23] This shift indicates a strong interaction between the $Ru(bpy)_3^{2+}$ and SWNT.[23,36]

Energy or charge-transfer mechanisms could be operating, in regard to quenching the $Ru(bpy)_3^{2+}$ excited state. Quenching of $*Ru(bpy)_3^{2+}$ luminescence by oxygen occurs via the electron- and energy-transfer mechanisms.[37] We assume that both of these mechanisms also participate in the quenching of $*Ru(bpy)_3^{2+}$−SWNT luminescence by air. Quenching of the $*Ru(bpy)_3^{2+}$ moiety in $*Ru(bpy)_3^{2+}$−SWNT by energy transfer to SWNT is possible because of the spectral overlap between the $*Ru(bpy)_3^{2+}$ emission and the SWNT absorption. However, direct illumination of the film with light, corresponding to $*Ru(bpy)_3^{2+}$ emission, did not change the conductivity of $Ru(bpy)_3^{2+}$−SWNT.

Both oxidative and reductive quenching of $*Ru(bpy)_3^{2+}$ luminescence have been observed for charge-transfer processes, depending on the driving force of the process.[38] Electron transfer from $*Ru(bpy)_3^{2+}$ to SWNT is thermodynamically allowed, with $\Delta G° = -1.14$ eV ($E°(Ru(bpy)_3^{3+}/*Ru(bpy)_3^{2+}) = -0.84$ V;[39] whereas for semiconducting SWNTs, $E° = +0.3$ V).[40] However, an oxidative quenching of $*Ru(bpy)_3^{2+}$ would decrease the number of holes, thus decreasing the photoconductivity of *p*-doped SWNTs, which was not observed in our experiments.

We conclude that the observed photoconductivity of $Ru(bpy)_3^{2+}$−SWNT films is indicative of electron transfer from SWNT to the photoexcited $Ru(bpy)_3^{2+}$, and that this is the major mechanism of luminescence quenching in $Ru(bpy)_3^{2+}$-modified SWNTs. The driving force for this process, $\Delta G° = -0.54$ eV ($E°(*Ru(bpy)_3^{2+}/Ru(bpy)_3^{+}) = 0.84$ V),[41] shows that the oxidation of SWNT by $*Ru(bpy)_3^{2+}$ is thermodynamically favorable.

We have used data on oxygen quenching of $Ru(bpy)_3^{2+}$ luminescence to estimate the quantum efficiency of electron transfer from SWNT to $*Ru(bpy)_3^{2+}$. Assuming that the oxygen quenching rate constant is the same for $*Ru(bpy)_3^{2+}$ and $*Ru(bpy)_3^{2+}$−SWNT, we have the following equation for the rate constant k_q for $*Ru(bpy)_3^{2+}$ quenching by SWNT:

$$\frac{\Delta I}{\Delta I^{SWNT}} \times \frac{I_{Ar}}{I_{air}} = \left(\frac{I_{Ar}}{I_{air}} + k_q\tau\right)(1 + k_q\tau)$$

where ΔI ($\Delta I = I_{Ar} - I_{air}$) and ΔI^{SWNT} ($\Delta I^{SWNT} = I_{Ar}^{SWNT} - I_{air}^{SWNT}$) are the oxygen-induced luminescence intensity change for $Ru(bpy)_3^{2+}$ and $Ru(bpy)_3^{2+}$−SWNT, respectively, and τ is the $Ru(bpy)_3^{2+}$ excited-state lifetime in the absence of the quencher.[42] From Figure 5, using $\tau = 6 \times 10^{-7}$ s,[43] we have $k_q = 2 \times 10^6$ s^{-1}. The quantum yield of formation of the $*Ru(bpy)_3^{2+}$ (ϕ_o) was determined to be unity.[44] Using the aforementioned values of k_q, τ, and ϕ_o, we find that the quantum yield ϕ of holes injection from $*Ru(bpy)_3^{2+}$ to SWNT is $\phi = \phi_o \times k_q\tau/(1 + k_q\tau) \approx 0.55$. This significant value of the quantum yield, together with the low rate of photogenerated hole decay, make $Ru(bpy)_3^{2+}$−SWNT films attractive for the construction of photon dose meters, for image storage, and other optoelectronic applications.[45−47]

The sensitivity of the $*Ru(bpy)_3^{2+}$−SWNT excited-state lifetime (τ) to redox quenching provides an opportunity for a conductivity-based detection of analytes. We have observed a 2-fold-faster increase of the photoconductivity of $Ru(bpy)_3^{2+}$−SWNT when the environment of the film was changed from air to argon. In contrast, the addition of 0.08 bar of NO_2, which is a strong oxidant of $*Ru(bpy)_3^{2+}$ ($E°(NO_2/NO_2^-) = 1.04$ V),[48] resulted in a 20-times-slower increase of the film conductivity.

In conclusion, we have demonstrated that photoinduced charge separation within chemically modified SWNTs results in persistent conductivity of semiconducting carbon nanotube films. Carboxylated SWNTs reveal negative persistent photoconductivity that could be quenched by infrared illumination. We have found that the covalent attachment of $Ru(bpy)_3^{2+}$ to SWNTs makes carbon nanotubes sensitive to light that is absorbed by $Ru(bpy)_3^{2+}$ and persistently photoconductive, thus opening opportunities for selective light control of conductivity of semiconducting SWNTs. Persistently photoconductive SWNTs have potential uses as nanosized optical switches, photodetectors, electro-optical information storage devices, and chemical sensors.

Acknowledgment. We are grateful to Prof. John Keller for useful conversations. This research was supported by the National Science Foundation (through Grant No. BES-0322455, to R.F.K.) and by DOD/DARPA/DMEA (under Award No. DMEA90-02-2-0216, to R.C.H.).

References and Notes

(1) Bachtold, A.; Hadley, P.; Nakanishi, T.; Dekker, C. *Science* **2001**, *294*, 1317.
(2) Keren, K.; Berman, R. S.; Buchstab, E.; Sivan, U.; Braun, E. *Science* **2003**, *302*, 1380.
(3) Postma, H. W. C.; Teepen, T.; Yao, Z.; Grifoni, M.; Dekker, C. *Science* **2001**, *293*, 76.
(4) Tans, S. J.; Verschueren, A. R. M.; Dekker, C. *Nature* **1998**, *393*, 49.
(5) Misewich, J. A.; Avouris, P.; Martel, R.; Tsang, J. C.; Heinze, S.; Tersoff, J. *Science* **2003**, *300*, 783.
(6) Collins, P. G.; Arnold, M. S.; Avouris, P. *Science* **2001**, *292*, 706.
(7) Fujiwara, A.; Matsuoka, Y.; Matsuoka, Y.; Suematsu, H.; Ogawa, N.; Miyano, K.; Kataura, H.; Maniwa, Y.; Suzuki, S.; Achiba, Y. *Carbon* **2004**, *42*, 919.
(8) Fujiwara, A.; Matsuoka, Y.; Suematsu, H.; Ogawa, N.; Miyano, K.; Kataura, H. *Jpn. J. Appl. Phys.* **2001**, *40*, L1229.
(9) Texter, J. *C. R. Chim.* **2003**, *6*, 1425.
(10) Gratzel, M. *Nature* **2001**, *414*, 338.
(11) Hurst, J. K.; Khairutdinov, R. F. In *Electron Transfer in Chemistry, Vol. 4—Catalysis of Electron Transfer, Heterogeneous, and Gas-Phase Systems*; Balzani, V., Ed.; Wiley: New York, 2001; p 578.
(12) Itkis, M. E.; Perea, D. E.; Niyogi, S.; Rickard, S. M.; Hamon, M. A.; Hu, H.; Zhao, B.; Haddon, R. C. *Nano Lett.* **2003**, *3*, 309.
(13) Kazaoui, S.; Minami, N.; Kataura, H.; Achiba, Y. *Synth. Met.* **2001**, *121*, 1201.
(14) Hennrich, F.; Wellmann, R.; Malik, S.; Lebedkin, S.; Kappes, M. M. *Phys. Chem. Chem. Phys.* **2003**, *5*, 178.
(15) http://www.carbonsolution.com.
(16) Rinzler, A. G.; Liu, J.; Dai, H.; Nikolaev, P.; Huffman, C. B.; Rodriguez-Macias, F. J.; Boul, P. J.; Lu, A. H.; Heymann, D.; Colbert, D. T.; Lee, R. S.; Fischer, J. E.; Rao, A. M.; Eklund, P. C.; Smalley, R. E. *Appl. Phys. A* **1998**, *67*, 29.
(17) Hu, H.; Zhao, B.; Itkis, M. E.; Haddon, R. C. *J. Phys. Chem. B* **2003**, *107*, 13838.
(18) Kus, P.; Knerr, G.; Czuchajowski, L. *J. Heterocyclic Chem.* **1990**, *27*, 7.
(19) Kus, P.; Knerr, G.; Czuchajowski, L. *J. Heterocyclic Chem.* **1990**, *27*, 1161.
(20) Peek, B. M.; Ross, G. T.; Edwards, S. W.; Meyer, G. J.; Meyer, T. J.; Erickson, B. W. *Int. J. Peptide Protein Res.* **1991**, *38*, 114.
(21) Hamon, M. A.; Hui, H.; Bhowmik, P.; Itkis, M. E.; Haddon, R. C. *Appl. Phys. A* **2002**, *74*, 333.
(22) Darken, L. S.; Hyder, S. A. *Appl. Phys. Lett.* **1983**, *42*, 731.
(23) Khairutdinov, R. F.; Itkis, M. E.; Haddon, R. C. *Nano Lett.* **2004**, *4*, 1529.
(24) We found that, under analogous illumination, resistance of a carboxylated SWNT film increased on ~2 kΩ.
(25) Lorenz, M. R.; Segal, B.; Woodbury, H. H. *Phys. Rev.* **1964**, *134*, 751.
(26) Nelson, R. J. *Appl. Phys. Lett.* **1977**, *31*, 351.
(27) Zeisel, R.; Bayerl, M. W.; Goennenwein, S. T. B.; Dimitrov, R.; Ambacher, O.; Brandt, M. S.; Stutzmann, M. *Phys. Rev. B* **2000**, *61*, R16283.
(28) Adachi, E. *J. Appl. Phys.* **1967**, *38*, 1972.
(29) Osquiguil, E.; Maenhoudt, M.; Wuyts, B.; Bruynseraede, Y.; Lederman, D.; Schuller, I. K. *Phys. Rev. B* **1994**, *49*, 3675.
(30) Linke, R. A.; Redmond, I.; Thio, T.; Chadi, D. J. *J. Appl. Phys.* **1998**, *83*, 661.

(31) Nieva, G.; Osquiguil, E.; Guimpel, J.; Maendhoudt, M.; Wuyts, B.; Bruynseraede, Y.; Maple, M. B.; Schuller, I. K. *Appl. Phys. Lett.* **1992**, *60*, 2159.

(32) Kudinov, V. I.; Kirilyuk, A. I.; Kreines, N. M.; Laiho, R.; Lähderanta, E. *Phys. Lett. A* **1990**, *151*, 358.

(33) Chadi, D. J.; Chang, K. J. *Phys. Rev. B* **1989**, *39*, 10063.

(34) Zervos, M.; Elliott, M.; Westwood, D. I. *Appl. Phys. Lett.* **1999**, *74*, 2026.

(35) Khairutdinov, R. F.; Zamaraev, K. I.; Zhdanov, V. P. *Electron Tunneling in Chemistry*; Elsevier: Amsterdam, 1989.

(36) Corni, S.; Tomasi, J. *J. Chem. Phys.* **2002**, *117*, 7266.

(37) Zhang, X.; Rodgers, M. A. J. *J. Phys. Chem.* **1995**, *99*, 12797.

(38) Lomoth, R.; Haupl, T.; Johansson, O.; Hammarstrom, L. *Chem. Eur. J.* **2002**, *8*, 102.

(39) Lin, C.-T.; Böttcher, M.; Chou, M.; Creutz, C.; Sutin, N. *J. Am. Chem. Soc.* **1976**, *98*, 6536.

(40) Kazaoui, S.; Minami, N.; Matsuda, N.; Kataura, H.; Achiba, Y. *Appl. Phys. Lett.* **2001**, *78*, 3433.

(41) Creutz, C.; Sutin, N. *Inorg. Chem.* **1976**, *15*, 496.

(42) Given that a collisional encounter between the quencher and the excited state is responsible for oxygen quenching, the ratio of the $Ru(bpy)_3^{2+}$ luminescence intensities of argon (I_{Ar}) and air (I_{air}) saturated solutions is given by the Stern−Volmer equation: $I_{Ar}/I_{air} = 1 + kc\tau$, where k is a quenching rate constant, c an oxygen concentration, and τ the $Ru(bpy)_3^{2+}$ excited-state lifetime in the absence of the quencher. If SWNT also quenches $Ru(bpy)_3^{2+}$ luminescence with a rate constant k_q, then for $Ru(bpy)_3^{2+}$−SWNT, we have $I_{Ar}/I_{air}^{SWNT} = 1 + kc\tau + k_q\tau$. After simple modification, we can easily get the following expression: $\Delta I/\Delta I^{SWNT} \times I_{Ar}/I_{air} = [(I_{Ar}/I_{air}) + k_q\tau](1 + k_q\tau)$.

(43) Hoffman, M. Z.; Bolletta, F.; Moggi, L.; Hug, G. L. *J. Phys. Ref. Data* **1986**, *18*, 219.

(44) Bolletta, F.; Juris, A.; Maestri, M.; Sandrini, D. *Inorg. Chim. Acta* **1980**, *44*, L175.

(45) Firszt, F.; Meczynska, H.; Legowski, S.; Zakrzewski, J.; Strzalkowski, K.; Wrobel, M. *Phys. Status Solidi C* **2004**, *1*, 916.

(46) Zardas, G. E.; Theodorou, D. E.; Euthymiou, P. C.; Symeonides, C. I.; Riesz, F.; Szentpall, B. *Solid State Commun.* **1998**, *105*, 77.

(47) Thio, T.; Bennett, J. W.; Chadi, D. J.; Linke, R. A.; Becla, P. *J. Cryst. Growth* **1996**, *159*, 345.

(48) Ram, M. S.; Stanbury, D. M. *Inorg. Chem.* **1985**, *24*, 2954.